ORGANOMETALLICS

Article

pubs.acs.org/Organometallics

Stoichiometric and Catalytic Solid−Gas Reactivity of Rhodium Bisphosphine Complexes

Sebastian D. Pike,[†] Tobias Krämer,[‡] Nicholas H. Rees,[†] Stuart. A. Macgregor,*[,‡] and Andrew S. Weller*[,†]

[†]Department of Chemistry, Chemistry Research Laboratories, Oxford University, Mansfield Road, Oxford OX1 3TA, U.K.

[‡]Institute of Chemical Sciences, Heriot-Watt University, Edinburgh, EH14 4AS, U.K.

Supporting Information

ABSTRACT: The complexes $[Rh(^{i}Bu_2PCH_2CH_2P^{i}Bu_2)L_2][BAr^{F}_4]$ [$L_2 = C_4H_6$, $(C_2H_4)_2$, $(CO)_2$, $(NH_3)_2$; $Ar^{F} = 3,5\text{-}C_6H_3(CF_3)_2$] have been synthesized by solid−gas reactivity via ligand exchange reactions with, in some cases, crystallinity retained through single-crystal to single-crystal transformations. The solid-state structures of these complexes have been determined, but in only one case ($L_2 = (NH_3)_2$) is the cation ordered sufficiently to enable its structural metrics to be determined by single crystal X-ray diffraction. The onward solid-state reactivity of some of these complexes has been probed. The bis-ammonia complex $[Rh(^{i}Bu_2PCH_2CH_2P^{i}Bu_2)(NH_3)_2][BAr^{F}_4]$ undergoes H/D exchange at bound NH_3 when exposed to D_2. The bis-ethene complex $[Rh(^{i}Bu_2PCH_2CH_2P^{i}Bu_2)(C_2H_4)_2][BAr^{F}_4]$ undergoes a slow dehydrogenative coupling reaction to produce a material containing a 1:1 mixture of the butadiene complex and a postulated mono-ethene complex. The mechanisms of these processes have been probed by DFT calculations on the isolated Rh cations. All the solid materials were tested as heterogeneous catalysts for the hydrogenation of ethene. Complexes with weakly bound ligands (e.g., $L_2 = (C_2H_4)_2$) are more active catalysts than those with stronger bound ligands (e.g., $L = (CO)_2$). Surface-passivated crystals, formed through partial reaction with CO, allow for active sites to be probed, either on the surface or the interior of the single crystal.

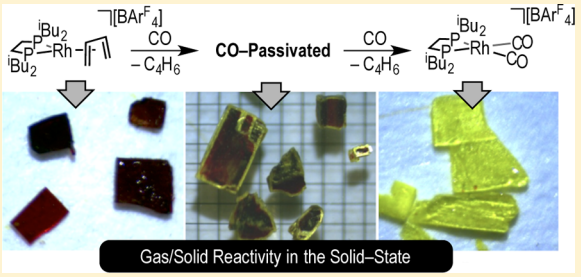

1. INTRODUCTION

While the study of organometallic complexes in the solution phase is widely explored,[1] investigation of their solid-state reactivity is less well-developed.[2−7] Potential advantages of reactivity in the solid-state lead from the constrained local environment that may influence selectivity and the lack of possibly deleterious solvent interactions. Indeed, for the isolation of highly reactive organometallic species, the solid state might be considered as the "perfect solvent" in that it offers a potentially noncoordinating environment. Demonstrating these advantages, we have recently reported the synthesis of σ-alkane complexes by a solid−gas route, e.g. $[Rh(^{i}Bu_2PCH_2CH_2P^{i}Bu_2)(NBA)][BAr^{F}_4]$ (**2**) [$Ar^{F}_4 = 3,5\text{-}C_6H_3(CF_3)_2$], in which a saturated norbornane (NBA) fragment coordinates with the metal center through two 3-center 2-electron interactions.[8,9] Complex **2** was generated in situ in a single-crystal to single-crystal (SC−SC) transformation by simple addition of H_2 to a crystalline norbornadiene (NBD) precursor, $[Rh(^{i}Bu_2PCH_2CH_2P^{i}Bu_2)(NBD)][BAr^{F}_4]$ (**1**), Scheme 1.

Ligand exchange reactions via solid−gas reactivity of organometallic complexes have been reported previously,[2,4,5,10] and sometimes these can be SC−SC transformations in which the crystallinity of the sample is retained throughout the reaction, allowing for characterization of the product directly by X-ray crystallography.[3,5,6,10−18] Typically these transitions occur with minimal disruption to the gross lattice, with often less than 4% change in unit-cell volume, although some examples report larger changes.[19−21]

Scheme 1. Solid−Gas Reaction to Form a σ-Alkane Complex, and the Eventual, Anion-Bound, Thermodynamic Product (S.S. = Solid-State; SC−SC = Single-Crystal to Single-Crystal)

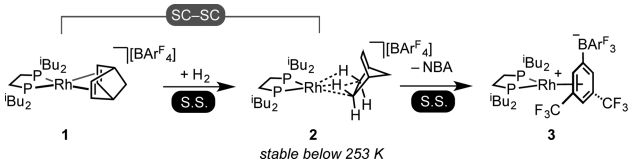

For the transformation of complex **1** to **2**, that retains crystallinity and only has a 1.5% change in unit-cell volume, we postulated that packing in the lattice is dominated by bulky $[BAr^{F}_4]^{-}$ anions which also form a defined octahedral cavity around **1** that is retained almost exactly in **2**. The anions thus have a dual role to play by defining the lattice and also allowing for structural change in the organometallic cation (i.e., NBD to NBA). Complex **2** is unstable at room temperature in the solid state, eventually forming the zwitterion $[Rh(^{i}Bu_2PCH_2CH_2P^{i}Bu_2)\{\eta^6\text{-}C_6H_3(CF_3)_2\}BAr^{F}_3]$, **3**, and free NBA, the thermodynamic products of the reaction.[8] However,

Received: December 22, 2014
Published: March 9, 2015

DOI: 10.1021/om5013133
Organometallics 2015, 34, 1487−1497

we posited that freshly prepared **2** could act as a suitable precursor for solid−gas reactivity, as the weakly bound alkane ligand could be easily displaced by an incoming ligand. In this contribution, we detail such reactivity with the exogenous ligands butadiene, ethene, CO, and NH_3 to form the corresponding adducts in the solid state and their onward reactivity. Some of these reactions are also SC−SC processes. We also document reactivity (H/D exchange, dehydrocoupling) and catalysis (hydrogenation of ethene) in these well-defined solid materials.

2. RESULTS AND DISCUSSION

2.1. Synthesis of Butadiene and Bis-ethene Complexes. The addition of 1,3-butadiene gas (∼4 atm) to freshly prepared crystalline **2** results in the rapid (∼1 min) formation of the dark-red/purple butadiene complex [Rh(^{i}Bu$_2$PCH$_2$CH$_2$P^{i}Bu$_2$)(η^4-C$_4$H$_6$)][BAr$^F_4$], **4**, with the concomitant release of one equivalent of NBA (Scheme 2) as measured

Scheme 2. Synthesis of Complex 4 by Solid-State and Solution Routes

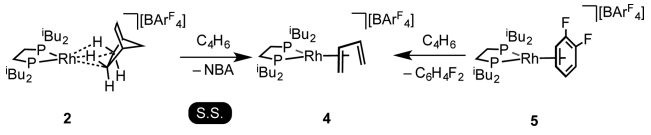

by ^{1}H NMR spectroscopy in CH_2Cl_2 solution. Complex **4** forms as an amorphous solid, i.e., this process is not a SC−SC transformation but can be conveniently recrystallized from 1,2-$C_6H_4F_2$/pentane to afford analytically pure material. Complex **4** can also be formed directly by solution routes by the addition of 1,3-butadiene gas to a 1,2-$C_6H_4F_2$ solution of [Rh(^{i}Bu$_2$PCH$_2$CH$_2$P^{i}Bu$_2$)(η^6-1,2-C$_6$H$_4$F$_2$)][BAr$^F_4$], **5**. The solution ^{1}H NMR spectrum (CD_2Cl_2) of **4** prepared by either route reveals three peaks of equal integration (δ 2.85, 4.27 and 5.44; 2 H each) attributed to the diene, which occur upfield in comparison to the ^{1}H NMR signals of free 1,3-C_4H_6 (δ (CCl_4) 5.03, 5.14, and 6.27),[22] consistent with coordination to a metal center. The solution ^{31}P{^{1}H} NMR spectrum shows a doublet (δ 54.6, J_{RhP} = 170 Hz). These data are similar to those reported for the closely related analogue [Rh(^{i}Pr$_2$PCH$_2$CH$_2$CH$_2$P^{i}Pr$_2$)(η^4-C$_4$H$_6$)][CF$_3$SO$_3$].[23] The solid-state ^{31}P{^{1}H} NMR spectrum shows a number of environments (i.e., more than 2), consistent with a disordered cation (vide infra and Supporting Information).

Addition of ethene gas to crystalline **2** forms a red, oily product assigned to the bis-ethene adduct [Rh(^{i}Bu$_2$PCH$_2$CH$_2$P^{i}Bu$_2$)(η^2-C$_2$H$_4$)$_2$][BAr$^F_4$], **6**, and free NBA as measured by solution NMR spectroscopy (Scheme 3).

Scheme 3. Formation of Complex 6 in the Solid-State and the Decomposition Reactions That Occur in Solution When Excess Ethene Is Not Present

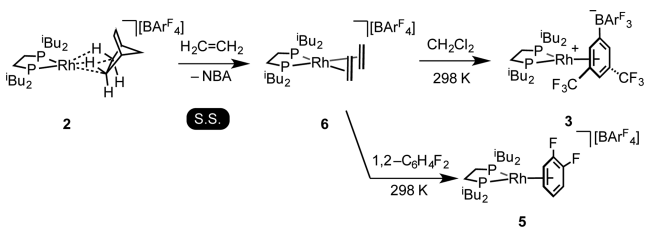

Analytically pure **6** can be generated by recrystallization from CH_2Cl_2/pentane while under 1 atm of ethene. Complex **6** is not stable at room temperature in solution in the absence of an ethene atmosphere. For example, in CH_2Cl_2 solution, decomposition to **3** occurs, whereas in 1,2-$C_6H_4F_2$ complex **5** forms, making solution-based routes less than ideal. By contrast, solid **6** does not lose ethene even when placed under a vacuum, as indicated by elemental microanalysis of a crystalline sample. That **6** is stable to vacuum in the solid-state suggests that ethene loss might proceed via an associative mechanism within the crystal and not by loss of ethene followed by coordination of an exogenous ligand. Similar observations have been made previously for the substitution of a dinitrogen ligand at a {Ir(POCOP)} fragment in the solid-state [POCOP = 2,6-bis(di-*tert*-butylphosphinito)benzene].[5]

The ^{1}H NMR spectrum of complex **6** at 240 K in CD_2Cl_2 reveals a sharp signal assigned to coordinated ethene (δ 3.98, fwhm = 7 Hz, relative integral 8 H),[24] while the ^{31}P{^{1}H} NMR spectrum at 240 K shows a doublet signal (δ 54.7, J_{RhP} = 144 Hz). At room temperature under four atmospheres of ethene, the ^{1}H NMR spectrum shows a broad signal assigned to free ethene (δ 5.31, fwhm = 49 Hz), with no separate peak observed for coordinated ethene, suggesting rapid exchange between coordinated and free ethene in solution. The ^{31}P{^{1}H} NMR spectrum displays a single environment essentially unchanged from that at 240 K. Warming to 298 K in the absence of ethene results in loss of ethene to form **3**. The solid-state ^{31}P{^{1}H} NMR spectrum shows two very broad environments, consistent with a disordered cation in the solid state (vide infra).

2.2. Synthesis of a Bis-carbonyl Complex by a Gas−Solid Reaction. Complexes such as **4** and **6** present ideal opportunities for solid-state reactivity, as the alkene ligands are likely to be relatively labile. Reaction with hydrogen in the solid state rapidly (less than 1 min) releases butane/ethane (observed by ^{1}H gas-phase NMR spectroscopy, see Supporting Information) with the concomitant formation of amorphous **3** as determined by ^{31}P{^{1}H} SSNMR spectroscopy, Scheme 4.

Scheme 4. Addition of H_2 to Complexes 4 or 6

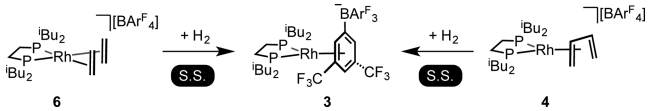

Presumably, the first formed alkane is lost from the metal center to result in [Rh(^{i}Bu$_2$PCH$_2$CH$_2$P^{i}Bu$_2$)]$^+$ coordinated with the [BAr$^F_4$]$^-$ anion, with the associated large structural change leading to the loss of crystallinity. By contrast, addition of CO gas (1 atm) to solid **4** or **6** forms bright yellow [Rh(^{i}Bu$_2$PCH$_2$CH$_2$P^{i}Bu$_2$)(CO)$_2$][BAr$^F_4$], **7**, with release of 1,3-butadiene or ethene into the head-space of the reaction vessel (a sealed NMR tube) and no loss of crystallinity (Figure 1). Complex **7** can also be produced by addition of CO gas to **5** in solution (1,2-$C_6H_4F_2$). The solution ^{31}P{^{1}H} NMR spectrum of **7** shows a single resonance (δ 56.1, J_{RhP} = 116 Hz). The ^{31}P{^{1}H} SSNMR spectrum also shows one environment, which is consistent with its solid-state structure (vide infra). The CO stretching frequencies in the IR spectra of **7** shows the anticipated two CO stretching bands (CH_2Cl_2, 2093.4 and 2049.1 cm^{-1}; ATR InfraRed, 2099.0 and 2056.9 cm^{-1}). These data are similar to closely related cationic Rh bis-

DOI: 10.1021/om5013133
Organometallics 2015, 34, 1487−1497

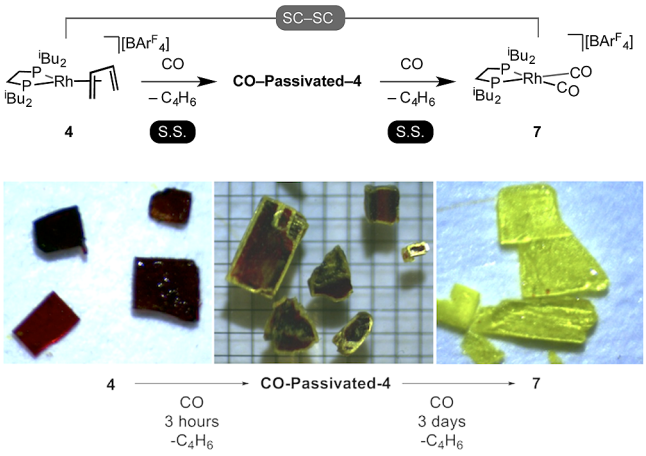

Figure 1. Reaction of **4** with CO in the solid state to form complex **7**. Optical microscope pictures of single crystals of **4**, **CO-Passivated-4** and **7** (bottom). Grid size = 0.5 mm.

carbonyl complexes, e.g., $[Rh(Cy_2PCH_2CH_2PCy_2)(CO)_2][BPh_4]$.[25]

This addition of CO gas (1 atm) to a single crystalline sample is slow, with full conversion to yellow **7** requiring ~3 days (for crystals of various sizes up to ~1 mm^3). Interestingly, the reaction occurs from the surface of the crystal inward, and an even layer of the yellow carbonyl complex forms on the faces of the crystal, as shown by optical microscopy (Figure 1). If the CO atmosphere is removed after 3 h, well-defined crystals result of **CO-Passivated-4** in which surface and near-surface sites are transformed into **7**. The ratio of **4**:**7** after 3 h, as determined by $^{31}P\{^1H\}$ SSNMR spectroscopy, was approximately 1:1, although this is dependent on the crystal size/surface area from batch to batch. Similar surface passivation using CO has been reported by Brookhart and co-workers, for solid–gas reactivity using the [Ir(POCOP)L] (L = N_2, CO).[5] A single-crystal X-ray diffraction experiment was conducted on the final crystalline product of this solid-state reaction of **4** with CO, i.e., **7**. These crystals appeared entirely yellow, retained their ability to rotate polarized light (which is often indicative of single crystallinity), and had unit cell parameters very similar to those of independently prepared **7** (vide infra). However, the mosaicity determined from the diffraction pattern was large and we were unable to solve the structure of the material produced via this solid-state route. The structure of **7**, as determined by crystals obtained by solution routes, is discussed in section 2.4. The bis-ethene complex **6** also reacts in the solid-state with CO to form **7**. In this case, the reaction takes only 3 h. The product of this reaction appears crystalline and diffracts with a single pattern, however, high mosaicity and cation disorder also did not allow the structure to be solved.

It is noteworthy that for a SC–SC transition to occur from **4** (or **6**) to **7**, not only must CO penetrate the crystal lattice but the gaseous butadiene (ethene) co-product must be able to escape without destroying the lattice. This suggests porosity within the crystalline network, which in some instances can come from loosely associated solvent that resides in channels in the crystal.[5] In the materials discussed herein, no co-crystallized solvent is present. It might well be that the CF_3 groups of the $[BAr^F_4]^-$ anions undergo a concerted motion that facilitates transport of CO and butadiene through the crystal, as has been recently suggested for reversible SC–SC transitions in Ag^+ coordination polymers which uptake alcohols.[21]

2.3. Synthesis of a Bis-ammonia Complex. Addition of ammonia gas to freshly prepared **2**, in the solid state, results in the formation of bis-ammonia complex $[Rh(^iBu_2PCH_2CH_2P^iBu_2)(NH_3)_2][BAr^F_4]$, **8**, alongside free NBA (Scheme 5). Crystallinity is lost in this reaction. Complex **8** can

Scheme 5. Synthesis of Complex 8 by Solid/Gas Reactions

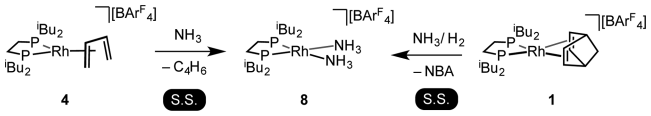

be recrystallized from 1,2-$C_6H_4F_2$/pentane solutions to afford crystals that were suitable for X-ray diffraction. To avoid traces of **3** in the final product, the direct addition of a mixture of NH_3 and H_2 to crystalline **1** was found to be the most effective way of synthesizing **8**. Ammonia complexes similar to **8** have been previously reported,[26–28] in particular the closely related $[Rh(dppe)(NH_3)_2]^+$.[29] Solution methods using 1,2-$C_6H_4F_2$ solvent were unsuccessful for the synthesis of **8** with decomposition to unidentified species occurring, even though complex **8** is stable in 1,2-$C_6H_4F_2$ solvent once formed by the solid-state route. Complex **8** can also be synthesized by the relatively rapid reaction (1 h) of solid **4** with NH_3 gas (with release of butadiene gas). Neither of these routes are SC–SC reactions, with the product forming as an amorphous solid, in contrast to the analogous reaction of **4** with CO. The $^{31}P\{^1H\}$ NMR spectrum of **8** solvated in 1,2-$C_6H_4F_2$ displays a doublet (δ 65.5, J_{RhP} = 177 Hz), similar to $[Rh(dppe)(NH_3)_2]^+$.[29] The ^1H NMR spectrum of **8** contains a sharp peak at δ 1.93 (relative integral 6 H) assigned to the coordinated ammine ligands. The proton chemical shift of ammine ligands is dependent upon hydrogen-bonding interactions with solvent or anion,[26] and in the case of **8** with a weakly coordinating anion in the weakly coordinating 1,2-$C_6H_4F_2$ solvent, the chemical shift observed is upfield of other reported values in similar complexes.[26] Complex **8** does not react with ethene in the solid state but does react with D_2, undergoing H/D exchange at the NH_3 ligand (Section 2.5).

2.4. Solid-State Structures. Single crystals of **4**, **6**, **7**, and **8** were prepared by solution recrystallization (see Supporting Information). For complexes **4**, **6**, and **7**, all three structures show significant disorder of the cation, which sits within an octahedral environment described by six, well-refined, $[BAr^F_4]^-$ anions. The cations in these structures were refined by use of similarity restraints to model the disorder components. In the case of complex **6**, the cation is disordered over two positions (~2:1 occupancy ratio) in which the corresponding two RhP_2 planes lie approximately perpendicular to each other (angle between planes 81°), and only the heavy atom positions (Rh and P) could be reliably resolved. The cation of **7** is also disordered over two positions (1:1 occupancy ratio), adopting a structure in which one cation is inverted relative to the other, and the RhP_2 planes are again perpendicular to each other. Each cation straddles a crystallographic mirror plane, and so the CO ligands in each cation are crystallographically equivalent. Figures 2A and B show this in detail. For **4**, refinement reveals four cation positions overlaid, with one rotated, one inverted, and one rotated and inverted relative to the original. These structures demonstrate the impact of rigid bulky anions upon relatively small cations: the anions dominate the packing structure and the cations may lie in a variety of thermodynami-

DOI: 10.1021/om5013133
Organometallics 2015, 34, 1487–1497

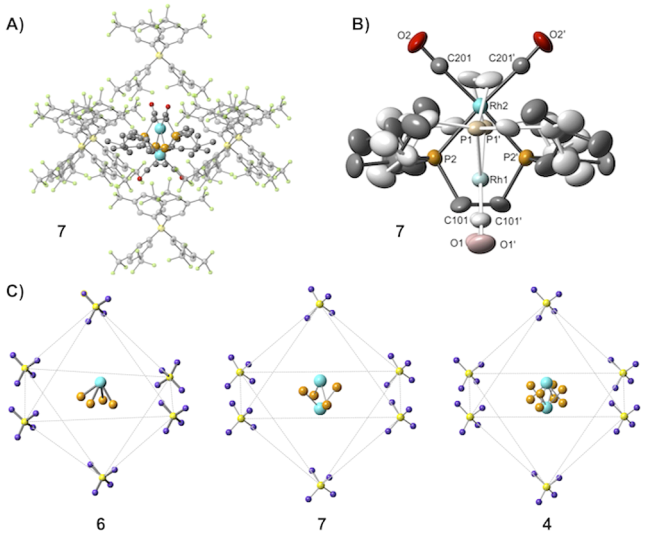

Figure 2. (A) Detailed view of the anion-cage and disordered components in complex **7** (ball and stick representation for simplicity, anions displayed as translucent, hydrogens atoms omitted). (B) Disordered cation in **7** (displacement ellipsoids at 30%, one disorder component displayed with pale atoms and bonds, hydrogens omitted). (C) Simplified packing diagrams of **6**, **7**, and **4**, showing disorder of the cation position. Cations are represented by $\{RhP_2\}$ only, anions represented as $\{BC_4\}$ only.

cally similar positions within the enclosed cavities.[30] Although the anions refine well in these structures the cation disorder means that comments on bond lengths and angles are not appropriate.

By contrast, the solid-state structure of **8** is well-ordered. However, unlike **4**, **6**, or **7**, the $[BAr^F{}_4]^-$ anions do not form a well-defined octahedron around the cation. Instead a distorted octahedron is observed in which one axial $[BAr^F{}_4]^-$ anion sits closer to the rhodium center than the others. This is demonstrated by consideration of the Rh−B vectors that lie approximately along crystallographic axes: ↑b 6.759(7) Å, ↓b 9.622(7) Å; a→ 9.593(1) Å, a← 9.593(1) Å; c→ 10.234(3) Å, c← 10.234(3) Å, Figure 3. This distortion along the b-axis may be influenced by hydrogen bonding between the ammine ligands and CF_3 groups on a proximal anion, as indicated by relatively close N−H···F distances [N(1)···F(190), 3.295(8) Å (H···F, 2.51 Å)].[31] Examples of hydrogen bonding in solid-state crystal structures of ammonia complexes have been reported,

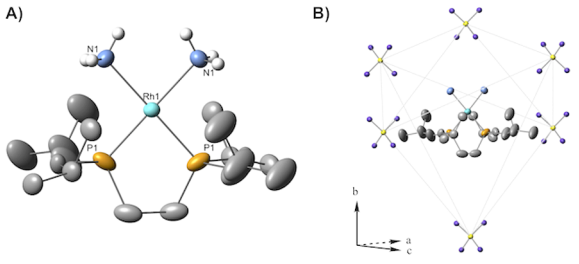

Figure 3. (A) Displacement ellipsoid plot (30% probability) for the cation of **8** in the solid-state. Hydrogen atoms (except those on ammine ligands) and anion omitted for clarity. (B) Crystal packing diagram of **8**, anion represented by BC_4 units (aryl groups omitted), and hydrogen atoms omitted for clarity. Selected bond length (Å) and angle (deg) data: Rh(1)−P(1), 2.2028(14); Rh(1)−N(1), 2.181(4); P(1)−Rh(1)−P(1′), 84.07(6); N(1)−Rh(1)−N(1′), 84.79(16).

often between N−H and an oxygen atom, and N···O distances vary from 2.84 to 3.19 Å (H···O, 2.00−2.37 Å).[26,27] The change in anion packing structure to accommodate N−H···F hydrogen bonds could also cause the loss of crystallinity upon transition from **4** to **8**. These hydrogen bonds also result in a cation that is not disordered, in contrast to, for example, **6**, in which the ethene ligands cannot engage in such interactions.

2.5. H/D Exchange in Complex 8. Microcrystalline samples of **8** react with D_2 in the solid state (48 h), or in 1,2-$C_6H_4F_2$ solution (24 h), to form $\mathbf{d_6}$**-8** with H/D exchange occurring exclusively at the ammine ligands (Scheme 6). When

Scheme 6. H/D Exchange upon Ammine Ligands in Solution or the Solid State

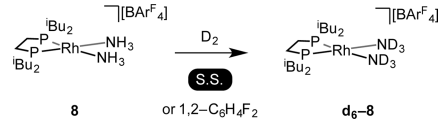

dissolved in 1,2-$C_6H_4F_2$, the ^{1}H NMR spectrum of $\mathbf{d_6}$**-8** reveals that the protio ammine signal observed for **8** [δ 1.93] is absent, while the ^{2}H NMR spectra contains a signal corresponding to the ND_3 ligands (δ 1.94). No signals indicating H/D exchange at the phosphine ligands were observed. No degradation of the crystal was observed during this process, as confirmed by X-ray crystallography. H/D exchange of bound ammonia has been previously reported in solution[32−34] and, most recently, within frozen argon matrices using $Ir(Cp^*)(H)_4$, however, in this case, a bound ammonia complex, $Ir(Cp^*)(H)_2(NH_3)$, was only implied by low temperature (10 K) IR spectroscopic studies.[35]

To elucidate the mechanism of H/D exchange in **8**, DFT calculations were employed to study H/H exchange between the ammine ligands of the isolated $[(^tBu_2PCH_2CH_2P^tBu_2)Rh(NH_3)_2]^+$ cation, **A**, with added H_2. The most accessible computed pathway is outlined in Figure 4, which shows free energies computed both in vacuo and corrected for 1,2-$C_6H_4Cl_2$ solvent (this being used in the absence of data for 1,2-$C_6H_4F_2$). Initial H_2 oxidative addition in solution proceeds with a computed barrier of 18.7 kcal/mol to give a Rh^{III} dihydride, **B** (G_{solv} = +3.3 kcal/mol). The NH_3 ligand *trans* to hydride in **B** is labilized (Rh···N = 2.27 Å) and so readily dissociates with a barrier of only 13.0 kcal/mol to give an isomer **C** (G_{solv} = +9.8 kcal/mol) in which it now H-bonds to the remaining ammine ligand. Rh−H/N−H exchange then proceeds through **TS(C−D)** at +22.8 kcal/mol, in which the outer-sphere NH_3 deprotonates the axial hydride (Rh···H^1 = 2.31 Å; N^2···H^1 = 1.08 Å) while simultaneously transferring a proton onto the equatorial hydride (H^a···H^1 = 1.51 Å; N^2···H^a = 1.08 Å).

Figure 4 shows the overall computed barrier for H/H exchange between cation **A** and H_2 is 22.8 kcal/mol, and it is apparent that the solvent correction reduces the barrier compared to the result in vacuo ($\Delta G^{\ddagger}_{vac}$ = 26.5 kcal/mol). This suggests increased charge separation in **TS(C−D)** compared to **A**, consistent with the involvement of a near-intact NH_4^+ cation in the former. Experimentally, H/D exchange occurs more rapidly in solution than in the solid state. While we have not attempted to model the solid-state environment here, the proximity of several fluorinated anions may produce a similar environment to that in solution, with a resultant reduction in barrier height. Alternative mechanisms for H/D exchange were also considered, including those based on initial oxidative addition of ammonia[36,37] or heterolytic

DOI: 10.1021/om5013133
Organometallics 2015, 34, 1487−1497

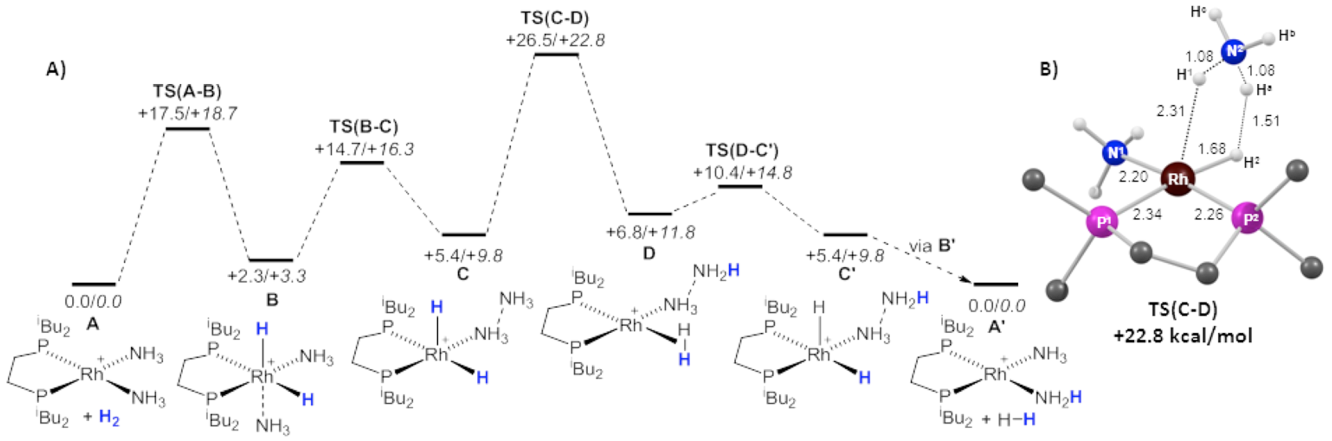

Figure 4. (A) Computed profile for H/H exchange via the reaction of $[(^{i}Bu_2PCH_2CH_2P^{i}Bu_2)Rh(NH_3)_2]^+$, **A**, with H_2. Relative free energies (kcal/mol) are reported in vacuo (plain text) and corrected for 1,2-$C_6H_4Cl_2$ solvent (in italics). H centers derived from the added H_2 molecule are highlighted in blue. (B) Computed structure of the Rh–H/N–H exchange transition state **TS(C–D)** with selected distances in Å. ^{i}Pr groups and nonparticipating H atoms on the chelating phosphine are omitted for clarity.

cleavage of H_2 over a Rh–NH_3 bond. These were both disfavored, however, the former entailing a barrier of 27.6 kcal/mol, while for the latter no intermediate incorporating an NH_4^+ cation could be located. Full details of these alternative pathways are given in the Supporting Information (see Figures S14–S17).

2.6. Solid–State Ethene Dehydrocoupling. Over a number of weeks at 298 K, orange/red single crystals of freshly prepared **6** change to a darker red/purple, becoming similar in color to freshly prepared complex **4**. When this material is dissolved in 1,2-$C_6H_4F_2$ solvent complex **4** is indeed observed in the $^{31}P\{^1H\}$ NMR spectrum, alongside the difluorobenzene adduct **5** (confirmed by ESI-MS). Complex **5** forms on dissolving **6** in 1,2-$C_6H_4F_2$ solvent (vide supra) and is thus a marker for this unstable bis-ethene complex or closely related complexes (Scheme 7). The transformation of **6** to **4** is

Scheme 7. Solid-State Ethene Dehydrocoupling and Subsequent Products Observed upon Solvation in 1,2-$C_6H_4F_2$ (L = Agostic or Solvent)

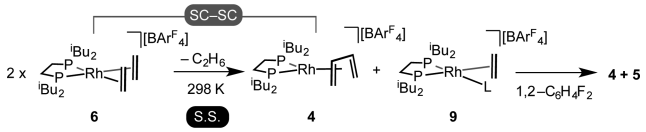

formally a dehydrocoupling of ethene. This transformation in the solid state was initially monitored over time by periodic sampling via dissolution in 1,2-$C_6H_4F_2$ of a solid sample kept 298 K. This showed a gradual increase in the proportion of complex **4** present and a decrease in **5**, with 40% conversion after 7 weeks (Figure 5). A sample kept for four months revealed ~50% conversion to **4**, this likely representing an upper limit for conversion. The color change of **6** to dark-red/purple occurs without apparent loss of crystallinity (by inspection of the sample using a polarizing microscope), and a single X-ray diffraction pattern could be collected. However, we were unable to solve the structure fully due to a highly disordered cation.

A sealed sample of **6** (NMR tube) releases ethane gas over several weeks as observed by gas-phase NMR spectroscopy. This observation is consistent with the conversion of **6** to **4**,

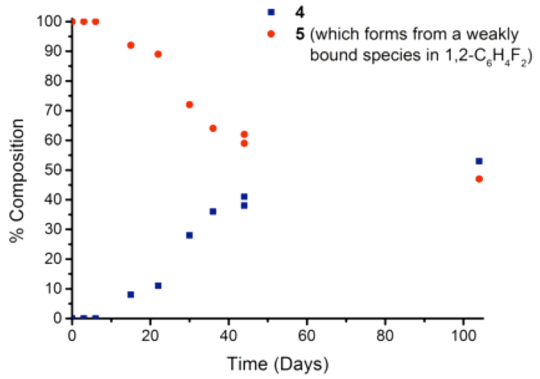

Figure 5. Formation of **4** from a solid sample of **6** as measured by integral of the $^{31}P\{^1H\}$ NMR signals of the products which form upon solvation in 1,2-$C_6H_4F_2$.

liberating one equivalent of hydrogen, which would then react with unreacted **6** to produce ethane gas (i.e., Scheme 4). It thus appears **6** converts to **4**, accompanied by sacrificial hydrogenation of one equivalent of ethene from a second molecule of **6**, also accounting for the apparent 50% maximum reaction conversion. Interestingly, crystallinity is retained during this process, which further suggests the sacrificial **6** does not lose ethene completely, as the resulting 12-electron fragment would likely form amorphous-**3** (Section 2.1). We suggest the formation of a 14-electron, 3-coordinate species $[Rh(^{i}Bu_2PCH_2CH_2P^{i}Bu_2)(\eta^2\text{-}C_2H_4)][BAr^F{}_4]$, **9**, in which only one ethene ligand is retained (Scheme 7) to account for the production of ethane. This species could be stabilized by an agostic interaction from the ^{i}Bu groups,[38] or by an interaction with the CF_3 groups from proximate anions in the lattice, and would likely form **5** on dissolution in 1,2-$C_6H_4F_2$. Budzelaar and co-workers have previously reported a related three-coordinate rhodium complex with a bidentate β-diiminate ligand and one alkene ligand.[39] Evidence for the formation of complex **9** comes from solvation (at 200 K, CD_2Cl_2) of a solid-sample sample of **6** that has been aged for two months. The $^{31}P\{^1H\}$ NMR spectrum recorded at this temperature reveals **4** to be the major product but less than 50% of the total integral, alongside signals for starting material **6** and its solution decomposition product **3**. Two new signals are also observed,

DOI: 10.1021/om5013133
Organometallics 2015, 34, 1487–1497

which are assigned to complex **9**, which couple to each other (^{31}P–^{31}P COSY experiment at 200 K), at δ 47.0 (J_{RhP} = 162 Hz, J_{PP} = 28 Hz); δ 71.4 (J_{RhP} = 186 Hz, J_{PP} = 28 Hz), Figure 6.

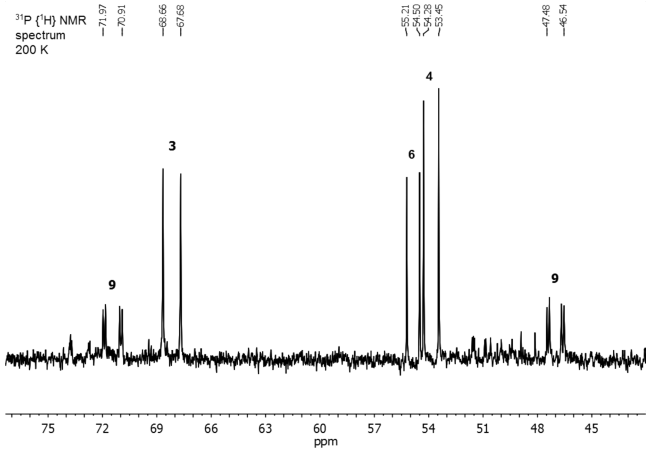

Figure 6. Low temperature ^{31}P{^{1}H} NMR spectrum (CD_2Cl_2, 200 K) of a solid sample of **6** that has been aged for 2 months.

One signal has a considerably larger J_{RhP} coupling constant, suggesting a weakly-bound *trans*-ligand (solvent or agostic interaction).[40] On warming to 250 K, complex **3** grows in at the expense of complex **9**.

SSNMR spectroscopy was also used to follow the solid-state transformation of **6** in situ. The ^{13}C{^{1}H} and ^{31}P{^{1}H} SSNMR spectra of freshly prepared complexes **4** and **6** were initially collected, and in keeping with their highly disordered solid-state structures, these spectra revealed multiple peaks for the signals related to the cation. For example, the ^{31}P{^{1}H} SSNMR spectrum of **4** shows a variety of closely spaced broad peaks, while that of **6** displays at least three broad phosphorus environments in the solid state, Figure 7. The ^{13}C{^{1}H} SSNMR

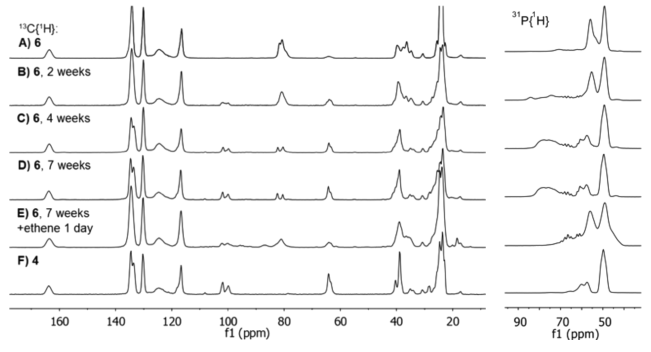

Figure 7. SSNMR spectra (^{13}C{^{1}H} left, ^{31}P{^{1}H} right) displaying the transformation of **6** over time (A–D) followed by the reaction of the products with ethene gas (E) at 298 K and a comparison with a pure sample of **6** (F).

spectra of **4** and **6** also show multiple peaks for the butadiene and ethene environments in their respective spectra, between 60–100 ppm. Monitoring a sample of **6** over the course of 6 weeks revealed the formation of complex **4** in both the ^{31}P{^{1}H} and ^{13}C{^{1}H} NMR spectra. In addition, a new signal (δ 82.4) slightly downfield to the ethene resonances in **6** was also observed in the ^{13}C{^{1}H} NMR spectrum, while the ^{31}P{^{1}H} SSNMR spectra show additional broad signals centered at δ 77 (Figure 7D). These signals are assigned to [Rh(^{i}Bu$_2$PCH$_2$CH$_2$P^{i}Bu$_2$)(η^2-C$_2$H$_4$)(L)][BAr$^{F}_4$], **9** (L = vacant site, agostic or anion interaction). On exposure to ethene gas, these additional signals disappear and **6** is reformed, consistent with the formulation of **9** as having a vacant, or masked, site (Figure 7E). When a sample of **6** was left at 323 K under an atmosphere of ethene (sealed NMR tube, 6 days), a small amount of 2-butene was observed. This could arise from isomerization of 1-butene, which would be formed by dimerization of ethene.[41] Under these conditions of temperature and excess ethene, no **4** is formed from the sample of **6**, with orange **6** recovered and a trace (~10%) of a complex characterized as a hexadiene adduct, **10**. Complex **10** was characterized by an independent synthesis from hexadiene and complex **5** (Supporting Information). Attempts to make the reaction turnover in a catalytic sense by increasing the temperature (e.g., 363 K) led to a partial melting of the crystalline material and no significant increase in the formation of coupled products.

The dehydrocoupling of ethene at rhodium centers to form butadiene complexes has been previously observed and mechanisms based on initial oxidative coupling or C–H bond activation have been proposed.[42−44] Such processes are also related to alkene oligomerization reactions.[45] Interestingly, the complex RhTp*(C$_2$H$_4$)$_2$ [Tp* = tris(3,5-dimethyl-1-pyrazol-1-yl)hydroborate] undergoes dehydrocoupling to give a butadiene complex in solution (with the concomitant release of ethane), but in the solid state, a hydrido-allyl species is formed.[44]

DFT calculations on isolated cations were again used to assess these different mechanistic possibilities and our favored pathway is outlined in Figure 8A. Starting from **E**,

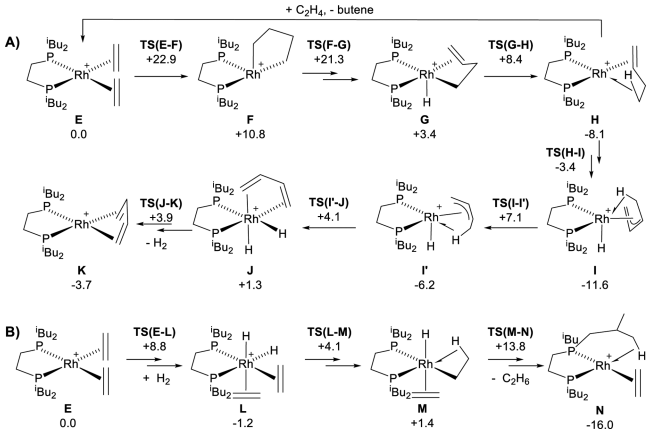

Figure 8. Free energy profiles (kcal/mol) for (A) the dehydrocoupling of ethene in [(^{i}Bu$_2$PCH$_2$CH$_2$P^{i}Bu$_2$)Rh(C$_2$H$_4$)$_2$]$^{+}$, **E**, and (B) hydrogenation of **E**. Several processes involve more than one step and these are indicated with a double arrow, and only the energy of the highest lying transition state between the two key minima is indicated. Full details of these and alternative mechanisms are available in the Supporting Information (see Figure S18–S24).

[(^{i}Bu$_2$PCH$_2$CH$_2$P^{i}Bu$_2$)Rh(C$_2$H$_4$)$_2$]$^{+}$ (i.e., the cation of **6**), oxidative coupling of ethene occurs with a barrier of 22.9 kcal/mol to give intermediate **F** (+10.8 kcal/mol). **F** exhibits a seesaw structure for which there are precedents with isoelectronic d^6 Ru(II) and Ir(III) centers.[46,47] β-H transfer then generates **G** from which facile C–H reductive coupling yields 1-butene complex **H** (−8.1 kcal/mol). Rearrangement and γ-H transfer then leads to hydrido-methylallyl intermediate

DOI: 10.1021/om5013133
Organometallics 2015, 34, 1487–1497

I at −11.6 kcal/mol.[48] **I** features a weak Rh···H−C agostic interaction and so could undergo H-transfer to form a *trans* dihydride intermediate (an isomer of **J**, see below, and Supporting Information, Figure S20). Instead a lower energy process involving facile rearrangement of the methylallyl ligand places the agostic *cis* to the hydride in isomer **I′** (−6.2 kcal/mol) from which H-transfer then gives **J** with *cis* hydrides and a *cis* η-C_4H_6 ligand. Dehydrocoupling is then completed via reductive elimination of H_2 to give **K** (the cation of **4**) at −3.7 kcal/mol.

Figure 8A shows the formation of **I** is thermodynamically favored over **K**, and so the facile, exergonic hydrogenation of **E** to **N** (modeling the cation of species **9** postulated experimentally) is required to drive the dehydrocoupling to completion (see Figure 8B: overall barrier = 13.8 kcal/mol; ΔG = −16.0 kcal/mol). The optimized structure of **N** features an agostic interaction between the Rh center and one of the ^{i}Bu methyl groups (see Supporting Information, Figure S11). The barrier energy span[49] of the dehydrocoupling profile (corresponding to **I** to **TS(M-N)**) is 25.4 kcal/mol, a value that is consistent with a slow dehydrocoupling process. The intermediacy of **H** is also consistent with the observation of 2-butene formed (after isomerization) in the presence of excess ethene.

Alternative dehydrocoupling mechanisms based on initial C−H activation to hydrido-alkenyl intermediates were also assessed. The C−H activation step ($\Delta G^{\ddagger}$ = 24.1 kcal/mol; ΔG = +19.3 kcal/mol) proved only slightly less accessible than the oxidative coupling; however, the onward reaction, either via ethene insertion into the Rh−alkenyl bond or insertion into the Rh−H bond involved transition states at 31.7 or 31.0 kcal/mol. Thus, these pathways have considerably higher barriers than the process based on oxidative coupling in Figure 8A. Full details of all alternative pathways are provided in the Supporting Information.

2.7. Solid-State Catalysis: Hydrogenation of Ethene. The complexes **1**−**8** were tested as solid-state catalysts for the hydrogenation of ethene. Such solid−gas reactivity has been reported before for organometallic catalysts in the solid state.[5,50−52] Gas-phase NMR spectroscopy was used to measure the hydrogenation of ethene in situ by the conversion of ethene to ethane. T_1 relaxation times for ethane and ethene in the gas phase were found to be similar for both species (ca. 0.6 s), as were their relative integrals with different acquisition delay times, suggesting that the relative integration of the two signals in to the gas-phase species is reliable. In a typical experiment, a high pressure NMR tube was loaded with (3 ± 0.3) mg (e.g., 2.2 × 10^{-3} mmol for **1**) of solid catalyst, and to this 1 atm (∼0.08 mmol) of ethene was added followed by ∼4 atm (∼0.31 mmol) of H_2. The progress of the reaction was monitored directly by integration of the gas-phase ^{1}H NMR spectra at 298 K.

Under these conditions of excess hydrogen, precatalysts containing alkene ligands (**1**, **4**, and **6**) all catalyze the reaction rapidly; for example, **1** requires less than 2 min to effect complete conversion (Figure 9). At the end of catalysis, when the ethene is fully consumed and hydrogen is still in excess, complex **3** is observed to be formed as characterized by ^{31}P{^{1}H} NMR spectra in CD_2Cl_2 solution, as there is no exogenous ligand to stabilize the metal center, consistent with the stoichiometric studies (section 2.1). This zwitterionic complex **3** is a very slow catalyst itself, only turning over ∼5% after 25 min, suggesting that dissociation, or η^6- to η^2-ring

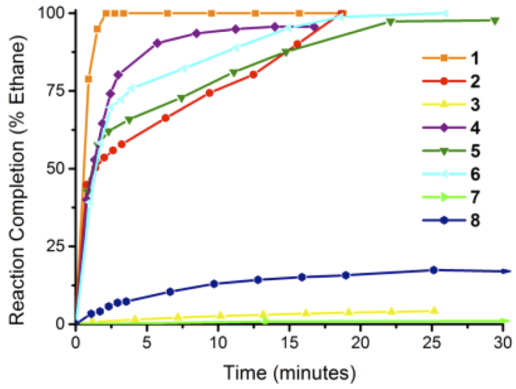

Figure 9. Hydrogenation of ethene to ethane using a variety of solid-state catalysts, 298 K. %Ethane conversion calculated from integrals of ethane and ethene signals by gas phase NMR spectroscopy.

slippage, of the anion to reveal a vacant site is a disfavored process in the solid state. This is a solid-state phenomenon, as in CH_2Cl_2 solution under an atmosphere of ethene **3** forms **6**, and hydrogenation of the bound alkene is then rapid (upon mixing). This also suggests that the resting state during catalysis in the solid state when using precatalysts such as **1** is unlikely to be **3**. Complex **7** is a very slow catalyst, showing essentially no turnover after 30 min, presumably as the carbonyl ligands are strongly bound. Complex **8** does show some activity (15% conversion after 30 min), perhaps suggesting that the ammine ligands are somewhat labile, consistent with the computational studies. In both of these cases, the organometallic species observed after completion of catalysis to the detection limit of solution ^{31}P{^{1}H} NMR spectroscopy is the same as the starting material, i.e., unchanged **7** and **8**. Interestingly, for precatalysts **2**, **5**, and **6**, the rate of hydrogenation, which is at first rapid, drops after around 2 min. This similar slower rate for all may be indicative of transformation of any surface organometallic species into a common species (possibly related to **3**) that turns over slowly. Also noteworthy is that this simple hydrogenation reaction occurs rapidly at ambient temperature (∼5 atm total pressure), while previous reports of the catalytic hydrogenation of ethene using solid-state organometallic catalysts typically require longer time scales and/or higher temperatures (albeit with lower pressure reaction conditions).[5,52,53]

As the surface area of a solid catalyst is likely to be important for the rate of catalysis, microcrystalline **1** was ground and separated into different particle size fractions using microsieves to give the following particle size regimes: less than 50 μm, 50−71 μm, and 71−150 μm. These materials were then subjected to catalytic hydrogenation of ethene using the standard conditions previously defined (i.e., 3.0 ± 0.3 mg of catalyst). Figure 10 shows that all the different size particles rapidly hydrogenate ethene with broadly similar temporal profiles over the first 10 min, promoting between 75 and 90% conversation. After a much longer time (16 h), all reached 100% conversion but at a much slower rate. Interestingly, the smaller particle sized catalysts appear to operate slightly faster as an ensemble, suggesting that the surfaces of the crystals are particularly active compared to the interior, or that smaller particle sizes allow for more rapid hydrogenation of the precatalyst. An alternative explanation is that the larger particle sizes of catalyst become deactivated sooner as there are relatively fewer active sites. As it might well be that all these factors are operating, possibly with a different temporal dependence depending on crystal size, and

DOI: 10.1021/om5013133
Organometallics 2015, 34, 1487−1497

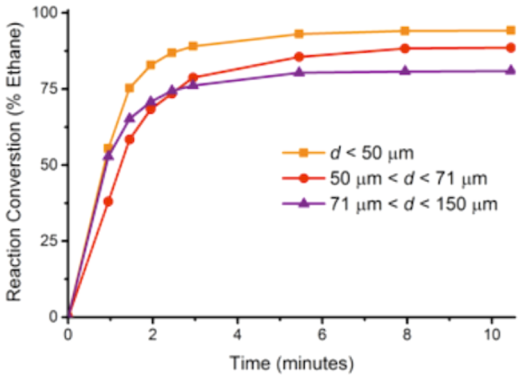

Figure 10. Hydrogenation of ethene using various particle size batches of solid **1** as a catalyst (starting conditions: 295 K, H_2 3.9 atm, ethene 1 atm).

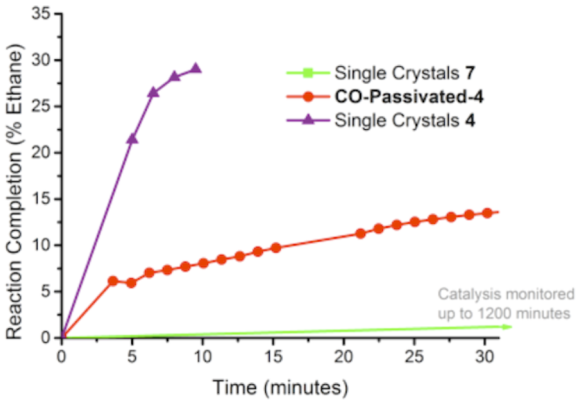

Figure 11. Hydrogenation of ethene using crystalline precatalysts. Ethene added at 1 atm, hydrogen added at less than 1 atm (~0.3 atm). Under these conditions, a maximum conversion of ~30% of ethane is achievable.

given the differences are relatively small, we are reluctant to speculate further with the current data.

2.8. Solid-State Catalysis: Passivation Studies. The data presented in the previous section suggest that catalysis might occur fastest upon the surface sites of the organometallic crystals. However, it is also likely that the metal centers located inside the interior of the crystal could be active by gas diffusion through the crystalline lattice. To probe this, we used **CO-Passivated-4**, an approach encouraged by the passivation techniques used by Brookhart and co-workers in studying alkene hydrogenation using [Ir(POCOP)$(H)_2$] systems.[5] As complex **7** essentially does not catalyze the hydrogenation of ethene, while **4** catalyzes the reaction rapidly (Figure 9), the **CO-Passivated-4** probes the ability of these interior metal sites to take part in catalysis. However, as complex **4** reacts with H_2 in the absence of ethene to, deleteriously, form **3**, in order to maintain single crystallinity, and thus the surface passivation of **CO-Passivated-4**, ethene is kept in excess with H_2 the limiting substrate in contrast to previously discussed catalysis in which hydrogen is in excess.

To baseline studies, complexes **4** and **7** were subjected to these conditions of catalysis in which hydrogen is the limiting substrate. A high pressure NMR tube containing (3 ± 0.3) mg of crystalline catalyst **7** was evacuated and refilled with ~1 atm of ethene and ~0.3 atm of H_2. As expected, single crystals of complex **7** are very poor catalysts for the hydrogenation of ethene under these conditions and only 3% conversion occurs within 1 h and little further progress is observed over the next 24 h (Figure 11). By contrast, single crystals of **4** hydrogenate ethene, until all hydrogen is consumed, in only ~9 min (i.e., 29% of ethene hydrogenated). These crystals retain their crystallinity and their ability to rotate polarized light. A second pressurization of hydrogen can be applied, and catalysis continues until the hydrogen is used up a second time (42% of ethene now being hydrogenated). Analysis of the resulting crystals by low temperature solution $^{31}P\{^1H\}$NMR spectroscopy (220 K, CD_2Cl_2) afterward showed that only **4** was present, and no **6** or **3** were resolved to the detection limit of ^{31}P NMR spectrocopy (~5%). This suggests that catalysis in the crystalline state occurs without significant involvement of the bulk crystal when ethene is in excess, with presumably only a small number of sites, likely on the surface, active for catalysis.

Under these conditions, **CO-Passivated-4** also catalyzes the hydrogenation of ethene but at a considerbly slower rate than pure crystalline **4**, with only 14% conversion reached after 33 min and the reaction only reaching completion after 12 h compared with the 10 min for **4** (Figure 11). After catalysis, the crystals appear intact and in good condition without significant cracking or change. A small trace of butane was observed in the gas phase ^1H NMR spectrum (~1% relative to the ethene signal), suggesting that a small proportion of the interior sites of **4** have been hydrogenated. A second amount of hydrogen can be subsequently added, and catalysis restarts. Low temperature $^{31}P\{^1H\}$ NMR spectroscopic analysis (220 K, CD_2Cl_2) of these crystals postcatalysis resolved only **4** and **7** to be present. This much slower rate of catalysis suggests that catalysis is mainly a surface process in these systems. However, that catalysis still does occur suggests that there is some penetration of ethene and hydrogen to access active interior sites of a crystal. These sites must be particularly active as no significant spectroscopic markers for their formation, i.e., **6** or **3** are observed. We cannot discount the possibility of crystal microcracking occurring (due to reaction with hydrogen and formation of **3**), which may expose the interior of the crystals.[54] Unfortunately, the remarkable selective hydrogenation of ethene in the presence of propene, demonstrated by Brookhart and co-workers using passivated single crystals, was not able to be reproduced with crystals of **CO-Passivated-4**.[5] Using a mixture of ethene, butene, and hydrogen (approximate 2:2:1 ratio), an approximately equal ratio of butane and ethane was produced in each case with crystalline catalysts of **4**, **CO-Passivated-4** and **7**, although the reaction rates varied dramatically as expected (**4** > **CO-Passivated-4** > **7**).

3. CONCLUSIONS

A number of solid-state reactions of well-defined organometallic complexes with gases are reported based upon the fragment [Rh(^{i}Bu$_2$PCH$_2$CH$_2$P^{i}Bu$_2$)][BAr$^F{}_4$]. In particular, we have shown that the σ-alkane complex **2** is a useful synthon for such solid-state synthesis, acting via a labile alkane ligand. This allows for the addition of gases such as ammonia and ethene to form the corresponding adducts, some of which, for example with ethene or NH_3, are not readily accessible via solution techniques. The corresponding butadiene complex, **4**, acts in a similar way by loss of alkene. Crystallinity may be maintained during some of these solid−gas ligand exchange reactions, when the crystal packing geometry remains similar in the starting materials and products (e.g., the displacement of ethene or butadiene ligands by CO). The crystal packing environments, which incorporate large [BAr$^F{}_4$]$^-$ anions that

DOI: 10.1021/om5013133
Organometallics 2015, 34, 1487−1497

provide a pseudo octahedral cavity in which the cations reside, can thus allow for subtle rearrangements in the solid state without disruption of the crystallinity or onward reactivity with the metal cation,[55] as we have noted previously.[8,9] In the solid state, these complexes can be used as precatalysts for the hydrogenation of ethene, show H/D exchange at bound NH_3 ligands, and promote ethene dehydrocoupling. Mechanisms for these last two processes are proposed on the basis of DFT calculations using molecular model systems, and modeling such reactivity in the solid state is the focus of current work. For catalysis, particle size and surface passivation experiments suggest that species on the surface act as the most active sites for catalysis rather than within the crystal. These observations encourage the use of solid-state organometallic chemistry in both synthesis and catalysis. Of course, in the latter, the identification of the actual active species/sites will likely be challenging as these might only represent a relatively small proportion of the bulk crystal.

4. EXPERIMENTAL SECTION

4.1. General Details. All manipulations, unless otherwise stated, were performed under an atmosphere of argon, using standard Schlenk-line and glovebox techniques. Glassware was oven-dried at 403 K overnight and flamed under vacuum prior to use. CH_2Cl_2, Et_2O, and pentane were dried using a Grubbs-type solvent purification system (MBraun SPS-800) and degassed by successive freeze−pump−thaw cycles.[56] CD_2Cl_2 and 1,2-$C_6H_4F_2$ were distilled under vacuum from CaH_2 and stored over 3 Å molecular sieves. Complexes **1**, **2**, **3**, and **5** were prepared according to previously described methods.[8] All other reagents were used as received from suppliers. Solution and gas-phase NMR spectra were recorded on Varian Unity 500 MHz, Bruker AVD 500 MHz, or Varian Mercury 300 MHz spectrometers at room temperature unless otherwise stated. Nondeuterated solvents were locked to a standard C_6D_6 solution. Residual protio solvent was used as reference for ^1H, ^2H, and ^{13}C NMR spectra in deuterated solvent samples. In 1,2-$C_6H_4F_2$, ^1H NMR spectra were referenced to the center of the downfield solvent multiplet (δ 7.07). ^{31}P NMR spectra were externally referenced to 85% H_3PO_4. All chemical shifts (δ) are quoted in ppm and coupling constants in Hz. Gas-phase samples were separately referenced to the reported values for hydrogen, ethane, ethene, and butadiene (all data were fully consistent with reported values).[52,57] SSNMR spectra were recorded on a Bruker Avance 3HD 400 MHz (University of Oxford) and Varian VNMRS 400 MHz (EPSRC National SSNMR Service, Durham University), using the cross-polarization pulse sequence (contact time 3−10 ms and recycle delay 1−2 s), with Spinal 64 or TPPM decoupling. A magic-angle spinning rate of 10 kHz was employed (under dry N_2). Spectral referencing is with respect to external neat tetramethylsilane for ^{13}C and to 85% H_3PO_4 for ^{31}P. Fourier Transform infrared (IR) spectroscopy was carried out using a Thermo-Scientific Nicolet iS5 with iD3 ATR and iD1 transmission attachments. Electrospray ionization mass spectrometry was recorded using a Bruker MicroTOF instrument directly connected to a modified Innovative Technology glovebox.[58]

4.2. Synthesis of [Rh(^{i}Bu$_2$PCH$_2$CH$_2$P^{i}Bu$_2$)(η^4-C$_4$H$_6$)][BAr$^F_4$] (4). [Rh(^{i}Bu$_2$PCH$_2$CH$_2$P^{i}Bu$_2$)(η^6-1,2-$C_6H_4F_2$)][BAr$^F_4$] (**5**) (250 mg, 0.179 mmol) was dissolved in 1,2-$C_6H_4F_2$ and the solution frozen and placed under vacuum. Butadiene gas was used to refill the flask and upon warming a color change to a dark-red/purple solution occurs, the flask was left sealed for 2 h. Because reducing the pressure inside the flask drives the backward reaction, releasing butadiene gas and the formation of **5**, complex **4** was recrystallized by adding pentane via syringe directly to the solution under an atmosphere of butadiene. Dark-red/purple crystalline material forms, 66% yield. Solid **4** is vacuum stable. Anal. Calcd for $C_{54}H_{58}BF_{24}P_2Rh$: C, 48.45; H, 4.37. Found: C, 48.57; H, 4.43. ESI-MS [M^+] calcd = 475.21, found [M^+] m/z = 475.21. ^1H NMR (500 MHz CD_2Cl_2): δ 0.94 [vt (^{i}Bu CH_3), J_{HH} = 7 Hz, 12H], 1.07 [d (^{i}Bu CH_3), J_{HH} = 7 Hz, 6H], 1.09 [d (^{i}Bu CH_3), J_{HH} = 7 Hz, 6H], 1.64 [m (^{i}Bu CH or CH_2), 4H], 1.74 [m (PCH_2CH_2P), 4H], 1.80−2.04 [m, (^{i}Bu CH or CH_2), 8H], 2.86 [d (C_4H_6), J_{HH} = 14 Hz, 2H], 4.27 [d (C_4H_6), J_{HH} = 7 Hz, 2H], 5.45 [m, (C_4H_6), 2H] 7.56 [s (BAr$^F_4$), 4H], 7.72 [s (BAr$^F_4$), 8H]. $^{31}P\{^1H\}$ NMR (202 MHz CD_2Cl_2): δ 54.64 [d, J_{RhP} = 170 Hz, 2P]. $^{31}P\{^1H\}$ SSNMR (161 MHz): δ 49.8 (br, major peak), 57.5 (br), 60.1 (br). $^{13}C\{^1H\}$ SSNMR (101 MHz): δ 22.7−36.2 [m (^{i}Bu CH_3, CH, PCH_2CH_2P), 14C], 38.0−40.6 [m (^{i}Bu CH_2), 4C], 63.5−64.2 [m (C_4H_6), 2C], 99.9−101.9 [m (C_4H_6), 2C], 116.7 [m (BAr$^F_4$), 8C], 124.6 [br (BAr$^F_4$), 8C], 130.3 [br (BAr$^F_4$), 8C], 133.6−134.6 [m (BAr$^F_4$), 4C], 163.8 [br (BAr$^F_4$), 4C].

Addition of butadiene (∼4 am) to preformed complex **2** (see below for insitu synthesis from complex **1**) resulted in the formation of complex **4** as an amorphous solid, which can be recrystallized from 1,2-$C_6H_4F_2$/pentane to give analytically pure material. See Supporting Information for crystallographic studies.

4.3. Synthesis of [Rh(^{i}Bu$_2$PCH$_2$CH$_2$P^{i}Bu$_2$)(C$_2$H$_4$)$_2$][BAr$^F_4$] (6). First, 26 mg (0.019 mmol) of solid [Rh(^{i}Bu$_2$PCH$_2$CH$_2$P^{i}Bu$_2$)($\eta^2\eta^2$-C_7H_8)][BAr$^F_4$] (**1**) was placed in a crystallization tube with a Young's tap and exposed to hydrogen (1 atm) for 10 min to form [Rh(^{i}Bu$_2$PCH$_2$CH$_2$P^{i}Bu$_2$)($\eta^2\eta^2$-C_7H_{12})][BAr$^F_4$] (**2**). Then the flask was evacuated, and ethene (1 atm) was immediately added. With the flask under a pressure of ethene, CH_2Cl_2 was added by syringe through a Suba-Seal to dissolve the compound forming a orange/red solution. Pentane was also added by syringe to form a layer over the CH_2Cl_2, and the flask was sealed under 1.5 atm of ethene. Orange/red crystals formed over 48 h, which could be isolated and appear vacuum stable (25% yield). The complex is not stable in solution (or when suspended in pentane) at room temperature in the absence of an ethene atmosphere, as decomposition to **3** occurs. Anal. Calcd for $C_{54}H_{60}BF_{24}P_2Rh$: C, 48.38; H, 4.51. Found: C, 48.52, H, 4.41. ^1H NMR (500 MHz CD_2Cl_2 240 K): δ 0.96 [d (^{i}Bu CH_3), J_{HH} = 6 Hz, 12H], 1.03 [d (^{i}Bu CH_3), J_{HH} = 6 Hz, 12H], 1.5−2.0 [br (^{i}Bu CH, ^{i}Bu CH_2 and PCH_2CH_2P), 16H], 3.98 [s (C_2H_4), 8H], 7.53 [s (BAr$^F_4$), 4H], 7.71 [s (BAr$^F_4$), 8H]. $^{31}P\{^1H\}$ NMR (202 MHz CD_2Cl_2 240 K):δ 54.74 [d, J_{RhP} = 144 Hz, 2P]. $^{31}P\{^1H\}$ SSNMR (161 MHz): δ 49.3 (br), 55.9 (br). $^{13}C\{^1H\}$ SSNMR (101 MHz): δ 22.5−25.6 [m (^{i}Bu CH_3), 8C], 30.5−39.6 [m (^{i}Bu CH, ^{i}Bu CH_2, PCH_2CH_2P), 10C], 80.7−81.6 [m (C_2H_4), 4C], 116.5 [m (BAr$^F_4$), 8C], 124.5 [br (BAr$^F_4$), 8C], 130.1 [br (BAr$^F_4$), 8C], 134.2 [br (BAr$^F_4$), 4C], 163.6 [br (BAr$^F_4$), 4C]. See Supporting Information for crystallographic studies.

4.4. Synthesis of [Rh(^{i}Bu$_2$PCH$_2$CH$_2$P^{i}Bu$_2$)(CO)$_2$][BAr$^F_4$] (7). [Rh(^{i}Bu$_2$PCH$_2$CH$_2$P^{i}Bu$_2$)(η^6-1,2-$C_6H_4F_2$)][BAr$^F_4$] (**5**) (30 mg, 0.022 mmol) was dissolved in CH_2Cl_2 and the solution frozen and placed under vacuum. CO gas was used to refill the flask, and upon warming, a slight color change from yellow/orange to bright-yellow occurred, and the flask was left sealed for 2 h. The solution was then degassed and crystallized by adding pentane (23 mg, 80% yield). Bright-yellow crystalline material formed. Anal. Calcd for $C_{52}H_{52}BO_2P_2F_{24}Rh$: C, 46.59; H, 3.91. Found: C, 46.67; H, 3.82. ESI-MS [M^+] calcd = 477.16, found [M^+] m/z = 477.16. IR spectroscopy (CH_2Cl_2 solution): CO stretches 2093.4 and 2049.1 cm^{-1}; (solid-state) CO stretches 2099.0 and 2056.9 cm^{-1}. ^1H NMR (300 MHz CD_2Cl_2): δ 1.12 [d (^{i}Bu CH_3), J_{HH} = 6 Hz, 12H], 1.16 [d (^{i}Bu CH_3), J_{HH} = 6 Hz, 12H], 1.89 [m (^{i}Bu CH), 4H], 1.96 [m (^{i}Bu CH_2), 8H], 2.10 [d, PCH_2CH_2P, J_{PH} = 18 Hz, 4H], 7.57 [s (BAr$^F_4$), 4H], 7.72 [s (BAr$^F_4$), 8H]. $^{31}P\{^1H\}$ NMR (122 MHz CD_2Cl_2):δ 56.10 [d, J_{RhP} = 116 Hz, 2P]. $^{31}P\{^1H\}$ SSNMR (161 MHz): δ 54.1 (br, 2P).

Alternatively, addition of CO gas (1 atm) to a single crystalline sample of complex **4** (∼30 mg) resulted in slow conversion to yellow **7** as monitored by ^{31}P SSNMR spectroscopy, with full conversion requiring 3−4 days depending on the crystal size. See Supporting Information for crystallographic studies on material produced via the solution route.

4.5. Synthesis of [Rh(^{i}Bu$_2$PCH$_2$CH$_2$P^{i}Bu$_2$)(NH$_3$)$_2$][BAr$^F_4$] (8). Solid [Rh(^{i}Bu$_2$PCH$_2$CH$_2$P^{i}Bu$_2$)($\eta^2\eta^2$-C_7H_8)][BAr$^F_4$] (**1**) (50 mg, 0.036 mmol) was placed in a Young's flask. The flask was degassed and placed under 1 atm NH_3 gas. The flask was then frozen in a liquid N_2 bath and opened to 1 atm pressure of H_2 while at low temperature.

DOI: 10.1021/om5013133
Organometallics 2015, 34, 1487−1497

The flask was then sealed and warmed; this generated roughly 1 atm NH_3 and 3 atm H_2. The solid quickly turned a bright-yellow color. The flask was left for 3 h. The product was washed twice with pentane to remove NBA. Crystals were grown from 1,2-$C_6H_4F_2$/pentane; 35 mg (0.027 mmol) produced; 73% yield. Anal. Calcd for $C_{50}H_{58}BP_2N_2F_{24}Rh$: C, 45.54; H, 4.43; N, 2.12. Found: C, 45.69; H, 4.43; N, 1.95. ^{1}H NMR (500 MHz 1,2-$C_6H_4F_2$): δ 1.18 [d (^{i}Bu CH_3), J_{HH} = 6 Hz, 12H], 1.33 [d (^{i}Bu CH_3), J_{HH} = 6 Hz, 12H], 1.51 [d (PCH_2CH_2P), J_{PH} = 14 Hz, 4H], 1.57 [m (^{i}Bu CH_2), 8H], 1.91 [m (^{i}Bu CH), 4H], 1.93 [s, NH_3, 6H], 7.68 [s (BAr^F_4), 4H], 8.32 [s (BAr^F_4), 8H]. ^{31}P{^{1}H} NMR (202 MHz 1,2-$C_6H_4F_2$): δ 65.45 [d, J_{RhP} = 177 Hz, 2P]. ^{31}P{^{1}H} SSNMR (161 MHz): δ 58.5 (vt, J_{RhP} = 155−170 Hz, 2P). See Supporting Information for crystallographic details.

4.6. Synthesis of [Rh(^{i}Bu$_2$PCH$_2$CH$_2$P^{i}Bu$_2$)(□^{4}-MeCH═CHCH═CHMe)][BAr$^F_4$] (10). First, 0.1 mL of previously degassed 2,4-hexadiene (mixture of isomers) was added to 5 mg (0.019 mmol) of solid [Rh(^{i}Bu$_2$PCH$_2$CH$_2$P^{i}Bu$_2$)(η^6-1,2-$C_6H_4F_2$)][BAr^F_4] (**5**) in an NMR tube. To this, 0.4 mL of CH_2Cl_2 was then added to solvate the mixture, causing a color change to bright red as **10** formed. **10** was crystallized by layering the solution with pentane (Yield 3 mg, 61%). Anal. Calcd for $C_{56}H_{62}BF_{24}P_2Rh$: C, 49.21; H, 4.57. Found: C, 49.35; H, 4.68. ^{1}H NMR (500 MHz CD_2Cl_2 240 K): δ 0.97 [d (^{i}Bu CH_3), J_{HH} = 6 Hz, 6H], 1.01 [d (^{i}Bu CH_3), J_{HH} = 6 Hz, 6H], 1.09 [d (^{i}Bu CH_3), J_{HH} = 6 Hz, 6H], 1.15 [d (^{i}Bu CH_3), J_{HH} = 6 Hz, 6H], 1.70 [m (^{i}Bu CH_2), 8H], 1.78−1.95 [br (^{i}Bu CH, PCH_2CH_2P, 2,4-C_4H_4**Me$_2$**), 14H], 3.98 [m (2,4-$C_4H_4Me_2$), 2H], 5.34 [d (2,4-$C_4H_4Me_2$), 2H]*, 7.56 [s (BAr^F_4), 4H], 7.72 [s (BAr^F_4), 8H] (*partially coincident with residual solvent peak, but confirmed by ^{1}H COSY NMR spectrum). ^{31}P{^{1}H} NMR (202 MHz CD_2Cl_2 240 K): δ 53.55 [d, J_{RhP} = 179 Hz, 2P]. ESI-MS [M^+] calcd = 503.24, found [M^+] m/z = 503.24. See Supporting Information for crystallographic details.

4.7. Catalysis: General Procedure. A high pressure NMR tube [volume ∼2 mL] was charged with (3 ± 0.3) mg (e.g., 2.2 × 10^{-3} mmol for **1**) of powdered microcrystalline catalyst (ground down with a spatula in the glovebox) and placed under ∼1 atm ethene. The tube was then frozen at 77 K, freezing the ethene, and H_2 was added in at 1 atm. When warmed to room temperature, this gave partial pressures of roughly 1 atm ethene (∼0.08 mmol) to 3.9 atm H_2 (∼0.31 mmol). Once warmed, the reaction was monitored immediately by gas phase ^{1}H NMR spectroscopy and the formation of ethane gas. See Supporting Information for more details.

4.8. Computational Details. Calculations were carried out with Gaussian 03 (revision D.01)[59] and Gaussian 09 (revision A.02)[60] Geometries were optimized without symmetry constraints employing the BP86 functional.[61,62] Rh and P centers were described with SDD relativistic ECPs[63] and associated basis sets, with d-orbital polarization added for P (ζ = 0.387).[64] 6-31G(d,p) basis sets[65,66] were used on all the remaining atoms. Stationary points were characterized via analytical second derivatives (minima, all positive eigenvalues; transition states, one imaginary eigenvalue), and free energies are reported at 298.15 K and 1 atm. IRC calculations and subsequent geometry optimizations confirmed the minima linked by each transition state. A correction for dispersion effects was included with Grimme's D3 parameter set,[67] while solvent effects were treated using the IEFPCM formalism in conjunction with Truhlar's SMD model.[68] In the absence of parameters for 1,2-*o*-difluorobenzene (ε_{exp} = 14), those for 1,2-*o*-dichlorobenzene (ε = 9.99) were employed. A comparison of reaction energies obtained with other solvents, fluorobenzene (ε = 5.42) and perfluorobenzene (ε = 2.03), is provided in the Supporting Information. Free energies of solvation were calculated at the same level of theory as described above (BP86/SDD/6-31G**).

■ ASSOCIATED CONTENT

Supporting Information

Full catalysis details, X-ray crystallography data collection and refinement, and computational details (PDF, XYZ, TXT). Full citation for ref 59 and 60. This material is available free of charge via the Internet at http://pubs.acs.org.

■ AUTHOR INFORMATION

Corresponding Authors

*For A.S.W.: E-mail: andrew.weller@chem.ox.ac.uk.
*For S.A.M.: E-mail: S.A.Macgregor@hw.ac.uk.

Notes

The authors declare no competing financial interest.

■ ACKNOWLEDGMENTS

We thank the EPSRC for funding via a DTP studentship (S.D.P.) and via grant number EP/K035908/1 (T.K.) as well as Johnson Matthey for the loan of rhodium salts. The EPSRC Solid-State NMR Spectroscopy Service at the University of Durham, UK, is thanked for acquisition of some of the ^{31}P NMR data.

■ DEDICATION

In memory of Professor Michael Lappert, a true pioneer and innovator in organometallic chemistry.

■ REFERENCES

(1) Hartwig, J. F. *OrganoTransition Metal Chemistry*; University Science Books: Sausalito, CA, 2010.
(2) Coville, N. J.; Cheng, L. *J. Organomet. Chem.* **1998**, *571*, 149−169.
(3) van der Boom, M. E. *Angew. Chem., Int. Ed.* **2011**, *50*, 11846−11848.
(4) Bianchini, C.; Peruzzini, M.; Zanobini, F. *Organometallics* **1991**, *10*, 3415−3417.
(5) Huang, Z.; White, P. S.; Brookhart, M. *Nature* **2010**, *465*, 598−601.
(6) Pike, S. D.; Weller, A. S. *Philos. Trans. R. Soc. A* **2015**, *373*, 20140187.
(7) Green, M. L. H.; Qin, J.; O'Hare, D. *J. Organomet. Chem.* **1988**, *358*, 375−388.
(8) Pike, S. D.; Thompson, A. L.; Algarra, A. s. G.; Apperley, D. C.; Macgregor, S. A.; Weller, A. S. *Science* **2012**, *337*, 1648−1651.
(9) Pike, S. D.; Chadwick, F. M.; Rees, N. H.; Scott, M. P.; Weller, A. S.; Krämer, T.; Macgregor, S. A. *J. Am. Chem. Soc.* **2015**, *137*, 820−833.
(10) Zenkina, O. V.; Keske, E. C.; Wang, R.; Crudden, C. M. *Angew. Chem., Int. Ed.* **2011**, *50*, 8100−8104.
(11) Bezzu, C. G.; Helliwell, M.; Warren, J. E.; Allan, D. R.; McKeown, N. B. *Science* **2010**, *327*, 1627−1630.
(12) Lim, S. H.; Olmstead, M. M.; Balch, A. L. *Chem. Sci.* **2013**, *4*, 311−318.
(13) Miller, E. J.; Brill, T. B.; Rheingold, A. L.; Fultz, W. C. *J. Am. Chem. Soc.* **1983**, *105*, 7580−7584.
(14) Xu, N.; Goodrich, L. E.; Lehnert, N.; Powell, D. R.; Richter-Addo, G. B. *Angew. Chem., Int. Ed.* **2013**, *52*, 3896−3900.
(15) Xu, N.; Powell, D. R.; Cheng, L.; Richter-Addo, G. B. *Chem. Commun.* **2006**, 2030−2032.
(16) Xu, N.; Powell, D. R.; Richter-Addo, G. B. *Angew. Chem., Int. Ed.* **2011**, *50*, 9694−9696.
(17) Ozerov, O. V.; Guo, C.; Papkov, V. A.; Foxman, B. M. *J. Am. Chem. Soc.* **2004**, *126*, 4792−4793.
(18) Weng, W.; Guo, C.; Moura, C.; Yang, L.; Foxman, B. M.; Ozerov, O. V. *Organometallics* **2005**, *24*, 3487−3499.
(19) Albrecht, M.; Lutz, M.; Schreurs, A. M. M.; Lutz, E. T. H.; Spek, A. L.; van Koten, G. *J. Chem. Soc., Dalton Trans.* **2000**, 3797−3804.
(20) Albrecht, M.; Lutz, M.; Spek, A. L.; van Koten, G. *Nature* **2000**, *406*, 970−974.
(21) Vitórica-Yrezábal, I. J.; Mínguez Espallargas, G.; Soleimannejad, J.; Florence, A. J.; Fletcher, A. J.; Brammer, L. *Chem. Sci.* **2013**, *4*, 696.
(22) *Spectral Database for Organic Compounds SDBS*; National Institute of Advanced Industrial Science and Technology: Tokyo; http://sdbs.db.aist.go.jp.

DOI: 10.1021/om5013133
Organometallics 2015, 34, 1487−1497

(23) Bosch, M.; Werner, H. *Organometallics* **2010**, *29*, 5646−5660.
(24) Krom, M.; Peters, T. P.; Coumans, R. G.; Sciarone, T. J.; Hoogboom, J.; ter Beek, S. I.; Schlebos, P. P.; Smits, J. M.; de Gelder, R.; Gal, A. W. *Eur. J. Inorg. Chem.* **2003**, *2003*, 1072−1087.
(25) Zotto, A. D.; Costella, L.; Mezzetti, A.; Rigo, P. *J. Organomet. Chem.* **1991**, *414*, 109−118.
(26) Burrows, A. D.; Michael, D.; Mingos, P.; E. Lawrence, S.; J. P. White, A.; J. Williams, D. *J. Chem. Soc., Dalton Trans.* **1997**, 1295−1300.
(27) Colquhoun, H. M.; Doughty, S. M.; Stoddart, J. F.; Williams, D. J. *Angew. Chem., Int. Ed.* **1984**, *23*, 235−236.
(28) Bengtsson, L. A.; Heaton, B. T.; Iggo, J. A.; Jacob, C.; Monks, G. L.; Ratnam, J.; Smith, A. K. *J. Chem. Soc., Dalton Trans.* **1994**, 1857−1865.
(29) Leitner, W.; Brown, J. M.; Brunner, H. *J. Am. Chem. Soc.* **1993**, *115*, 152−159.
(30) Inokuma, Y.; Kawano, M.; Fujita, M. *Nature Chem.* **2011**, *3*, 349−358.
(31) Spek, A. *J. Appl. Cryst.* **2003**, *36*, 7−13.
(32) Koelliker, R.; Milstein, D. *J. Am. Chem. Soc.* **1991**, *113*, 8524−8525.
(33) Jungton, A.-K.; Kläring, P.; Braun, T.; Eißler, A. *Z. Anorg. Allg. Chem.* **2012**, *638*, 505−511.
(34) Khaskin, E.; Iron, M. A.; Shimon, L. J. W.; Zhang, J.; Milstein, D. *J. Am. Chem. Soc.* **2010**, *132*, 8542−8543.
(35) Jungton, A.-K.; Herwig, C.; Braun, T.; Limberg, C. *Chem.—Eur. J.* **2012**, *18*, 10009−10013.
(36) Macgregor, S. A. *Organometallics* **2001**, *20*, 1860−1874.
(37) Zhao, J.; Goldman, A. S.; Hartwig, J. F. *Science* **2005**, *307*, 1080−1082.
(38) Luo, X.-L.; Kubas, G. J.; Burns, C. J.; Butcher, R. J.; Bryan, J. C. *Inorg. Chem.* **1995**, *34*, 6538−6545.
(39) Budzelaar, P. H. M.; Moonen, N. N. P.; de Gelder, R.; Smits, J. M. M.; Gal, A. W. *Chem.—Eur. J.* **2000**, *6*, 2740−2747.
(40) Pregosin, P. S. *NMR in Organometallic Chemistry*; Wiley−VCH: Weinheim, 2012.
(41) Exposure of a crystalline sample of **6** or **4** to 1-butene results in the isomerizarion to 2-butene, as measured by gas-phase ^{1}H NMR spectroscopy. By IR spectroscopy, this is a mixture of *cis*- and *trans*-2-butene. See Supporting Information.
(42) Dudle, B.; Blacque, O.; Berke, H. *Organometallics* **2012**, *31*, 1832−1839.
(43) Chin, C. S.; Lee, H.; Noh, S.; Park, H.; Kim, M. *Organometallics* **2003**, *22*, 2119−2123.
(44) Paneque, M.; Pérez, P. J.; Pizzano, A.; Poveda, M. L.; Taboada, S.; Trujillo, M.; Carmona, E. *Organometallics* **1999**, *18*, 4304−4310.
(45) Agapie, T.; Labinger, J. A.; Bercaw, J. E. *J. Am. Chem. Soc.* **2007**, *129*, 14281−14295.
(46) Scott, N. M.; Pons, V.; Stevens, E. D.; Heinekey, D. M.; Nolan, S. P. *Angew. Chem., Int. Ed.* **2005**, *44*, 2512−2515.
(47) Huang, D.; Streib, W. E.; Bollinger, J. C.; Caulton, K. G.; Winter, R. F.; Scheiring, T. *J. Am. Chem. Soc.* **1999**, *121*, 8087−8097.
(48) Nicasio, M. C.; Paneque, M.; Pérez, P. J.; Pizzano, A.; Poveda, M. L.; Rey, L.; Sirol, S.; Taboada, S.; Trujillo, M.; Monge, A.; Ruiz, C.; Carmona, E. *Inorg. Chem.* **1999**, *39*, 180−188.
(49) Kozuch, S.; Shaik, S. *Acc. Chem. Res.* **2010**, *44*, 101−110.
(50) Bianchini, C.; Farnetti, E.; Graziani, M.; Kaspar, J.; Vizza, F. *J. Am. Chem. Soc.* **1993**, *115*, 1753−1759.
(51) Siedle, A. R.; Newmark, R. A. *Organometallics* **1989**, *8*, 1442−1450.
(52) Matthes, J.; Pery, T.; Gründemann, S.; Buntkowsky, G.; Sabo-Etienne, S.; Chaudret, B.; Limbach, H.-H. *J. Am. Chem. Soc.* **2004**, *126*, 8366−8367.
(53) Bianchini, C.; Frediani, P.; Graziani, M.; Kaspar, J.; Meli, A.; Peruzzini, M.; Vizza, F. *Organometallics* **1993**, *12*, 2886−2887.
(54) Oliván, M.; Marchenko, A. V.; Coalter, J. N.; Caulton, K. G. *J. Am. Chem. Soc.* **1997**, *119*, 8389−8390.
(55) Pike, S. D.; Weller, A. S. *Dalton Trans.* **2013**, *42*, 12832−12835.
(56) Pangborn, A. B.; Giardello, M. A.; Grubbs, R. H.; Rosen, R. K.; Timmers, F. J. *Organometallics* **1996**, *15*, 1518−1520.
(57) Zuschneid, T.; Fischer, H.; Handel, T.; Albert, K.; Häfelinger, G. *Z. Naturforsch. B* **2004**, *59b*, 1153−1176.
(58) Lubben, A. T.; McIndoe, J. S.; Weller, A. S. *Organometallics* **2008**, *27*, 3303−3306.
(59) Frisch, M., et al. *Gaussian 03*, revision D.01; Gaussian, Inc.: Wallingford, CT, 2004.
(60) Frisch, M., et al. *Gaussian 09*, revision A.02; Gaussian, Inc.: Wallingford, CT, 2013.
(61) Becke, A. D. *Phys. Rev. A* **1988**, *38*, 3098−3100.
(62) Perdew, J. P. *Phys. Rev. B* **1986**, *33*, 8822−8824.
(63) Andrae, D.; Häußermann, U.; Dolg, M.; Stoll, H.; Preuß, H. *Theor. Chim. Acta* **1990**, *77*, 123−141.
(64) Höllwarth, A.; Böhme, M.; Dapprich, S.; Ehlers, A. W.; Gobbi, A.; Jonas, V.; Köhler, K. F.; Stegmann, R.; Veldkamp, A.; Frenking, G. *Chem. Phys. Lett.* **1993**, *208*, 237−240.
(65) Hehre, W. J.; Ditchfield, R.; Pople, J. A. *J. Chem. Phys.* **1972**, *56*, 2257−2261.
(66) Hariharan, P. C.; Pople, J. A. *Theor. Chim. Acta* **1973**, *28*, 213−222.
(67) Grimme, S.; Antony, J.; Ehrlich, S.; Krieg, H. *J. Chem. Phys.* **2010**, *132*, 154104.
(68) Marenich, A. V.; Cramer, C. J.; Truhlar, D. G. *J. Phys. Chem. B* **2009**, *113*, 6378−6396.

DOI: 10.1021/om5013133
Organometallics 2015, 34, 1487−1497